

Design and reactivity of pentapyridyl metal complexes for ammonia oxidation

Samantha I. Johnson, Spencer P. Heins, Christina M. Klug, Eric S. Wiedner, R. Morris Bullock, Simone Raugei

Center for Molecular Electrocatalysis, Pacific Northwest National Laboratory, P.O. Box 999, Richland, Washington 99352, United States

Table of Contents

Computational Methods.....	S-2
Table S1. All N-H bond dissociation free energies for M(PY5) complexes. BDFEs reported in kcal/mol.....	S-3
Molecular Orbital Diagrams	S-4
Figure S1. Metal <i>d</i> orbitals split into the octahedral σ ligand field, as shown above. Mixing with the π orbitals, as shown in the nitride complex, breaks the degeneracy of the e_g and t_{2g} sets.	S-4
This figure is adapted from Nugent and Mayer ¹³	S-4
Figure S2. Filling these orbitals in the C_{4v} ligand field is shown for both Mo and Ru.	S-4
Release of other NH_x complexes	S-5
Table S2. All free energies for hydrazine and diazine formation. Energies in kcal/mol.....	S-5
Scheme S1. Two Fe(PY5) amido complexes can couple to form the μ_2 -hydrazido complex. Energy in kcal/mol.....	S-6
Scheme S2. Two [(PY5)Mo-N] ⁺² molecules can couple to form a bridging μ -N ₂ complex. This is sensitive to solvent. Energies in kcal/mol.....	S-6
Table S3. Free energies to couple and release N ₂	S-6
Modified PY5 ligands	S-7
Figure S3. Modified PY5-X ligand, where X = NH ₂ , H, and CF ₃	S-7
Figure S4. a. Gas-phase electronic energy change and b. Solution phase electronic energy for the coupling vs. the amount of π^* character of the nitride ligand.	S-8

Table S5. All reported complexes, their π^* character, solution phase formation of the $\mu\text{-N}_2$ complexes, and electronic and solution phase energies to couple and evolve N_2	S-9
Geometries	S-10
Experimental Procedures	S-11
NMR Spectra	S-14
Apparatus for Headspace Sampling of J. Young Tubes	S-18
Gas Chromatograms.....	S-19
Results of N_2 Quantification	S-26
References.....	S-27

Computational Methods

Structures were optimized using the B3LYP functional^{1,2} in the gas phase, with the 6-31G** basis set for C, N, O and H^{3,4} and the Stuttgart-Dresden basis set and relativistic effective core potential (SDD)⁵ for the metal centers. The Grimme D2 dispersion correction was used in all calculations.⁶ Harmonic vibrational frequency calculations at the same level of theory were performed to obtain thermal and zero point energy (ZPE) corrections. Single point solvation calculations using the charge density-based continuum solvent (SMD) model⁷ in acetonitrile. Free energies are reported at the standard state condition of $T = 298.15$ K and $p = 1$ atm NH₃. The solvation energy of acetonitrile in acetonitrile was computed by first calculating the 1 atm gas phase free energy of acetonitrile and then correcting it by the empirical free energy of vaporization of 1.27 kcal/mol.⁸ These calculations were carried out using Gaussian 09.⁹ Further electronic structure calculations were completed using the standalone NBO 6.0¹⁰ program from input files generated by Gaussian 09. For the dimeric complexes, gas phase energies were calculated again with the 6-31G** basis set for C, N, O and H^{3,4} and the def2-SVP basis set and ECP^{5,11} for metals in Orca 4.0¹². For solvated calculations, again the SMD model was used. These methods have been successfully used in other computational studies of ammonia oxidation and nitrogen reduction.^{13,14}

Table S1. All N-H bond dissociation free energies for M(PY5) complexes. BDFEs reported in kcal/mol.

M	S_{M-NH_3}	First BDFE	S_{M-NH_2}	Second BDFE	S_{M-NH}	Third BDFE	S_{M-N}
Cr	2	64.9	$^5/2$	94.5	1	74.0	$^1/2$
Mo	1	68.1	$^3/2$	64.8	0	64.0	$^1/2$
W	1	64.2	$^5/2$	54.9	0	67.0	$^1/2$
Mn	$^5/2$	96.1	2	102.3	$^1/2$	72.8	0
Fe	0	88.1	$^5/2$	103.5	1	84.8	$^1/2$
Ru	0	88.0	$^1/2$	99.1	1	75.8	$^1/2$
Os	0	83.2	$^1/2$	96.3	1	71.4	$^1/2$

Molecular Orbital Diagrams

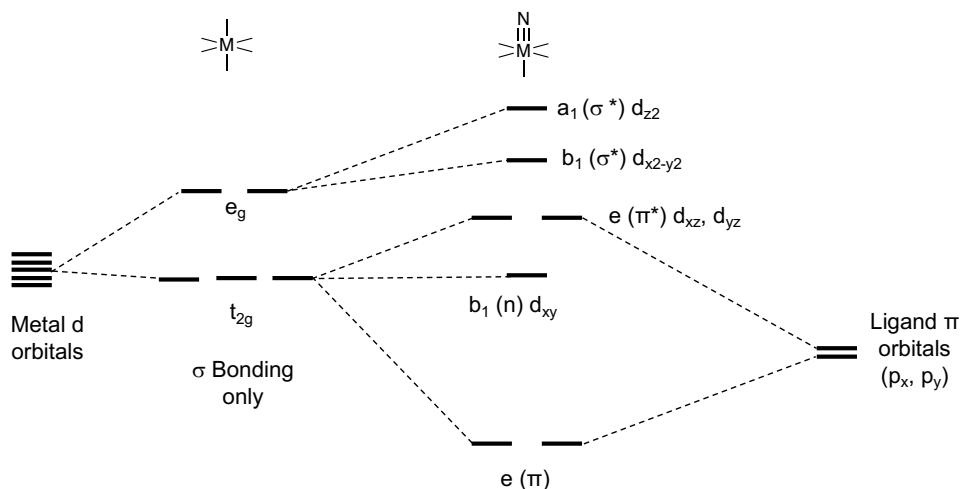


Figure S1. Metal d orbitals split into the octahedral σ ligand field, as shown above. Mixing with the π orbitals, as shown in the nitride complex, breaks the degeneracy of the e_g and t_{2g} sets.

This figure is adapted from Nugent and Mayer¹⁵.

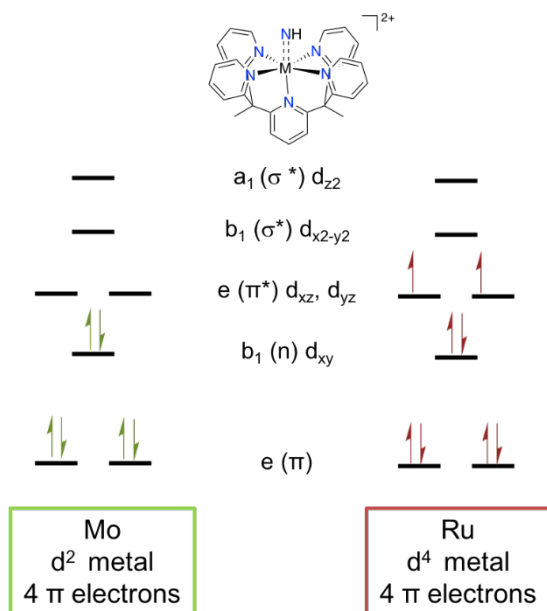


Figure S2. Filling these orbitals in the C_{4v} ligand field is shown for both Mo and Ru.

Release of other NH_x complexes

Various M-NH_x intermediates along the HAT removal pathway can homocouple. For example, if two amides couple, in principle, they could release hydrazine. Similarly, two imides could release diazine, though it would be unstable. The reactions can be seen in equations S1, with the energetics for various metals reported in Table S2.

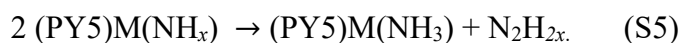
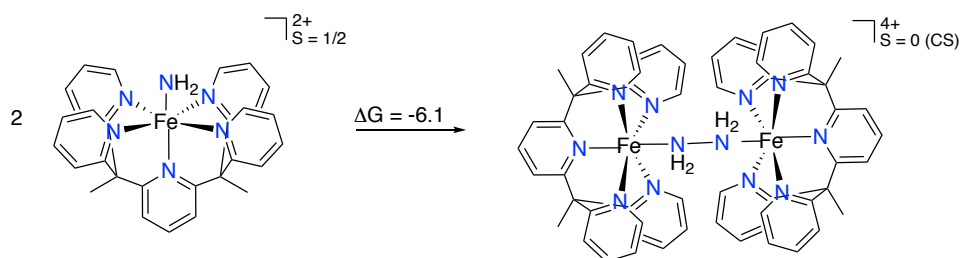


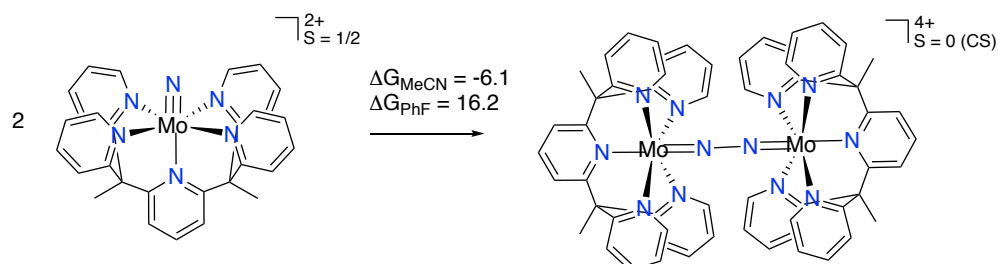
Table S2. All free energies for hydrazine and diazine formation. Energies in kcal/mol.

M	Hydrazine release	Diazine release
Cr	109.8	-23.8
Mo	99.5	25.4
W	107.5	53.2
Mn	77.8	-56.3
Fe	-22.7	-93.6
Ru	-22.7	-84.8
Os	69.3	-67.9

For hydrazine release, the only metals with favourable thermodynamics are Fe and Ru. To explore this possibility, the energy of formation of the bridged Fe hydrazido complex was calculated to be -6.1 kcal/mol. This is shown in Scheme S1. While this was favourable, the high BDFE required to achieve this state made it less promising. In the diazine release, all complexes with exergonic formation of diazine also had endergonic HAT to ArO•, rendering them unusable in this application.



Scheme S1. Two Fe(PY5) amido complexes can couple to form the μ_2 -hydrido complex. Energy in kcal/mol.



Scheme S2. Two $[(\text{PY}5)\text{Mo-N}]^{2+}$ molecules can couple to form a bridging $\mu\text{-N}_2$ complex. This is sensitive to solvent. Energies in kcal/mol.

Equation 1 shows two nitrido complexes coupling, evolving N_2 , and binding NH_3 to complete a catalytic cycle.

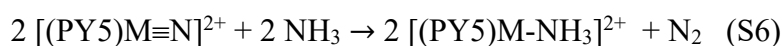


Table S3. Free energies to couple and release N_2

$[(\text{PY}5)\text{M}(\text{N})]^{+2}$	Free energy to couple and release N_2 in MeCN (eq. 1) [kcal/mol]
Cr	-108.6
Mn	-134.7
Fe	-194.4
Mo	-35.5
Ru	-167.4
W	-13.7
Os	-143.7

Modified PY5 ligands

PY5 ligands were modified in the *para* position of the apical pyridine to probe the role of the *trans* effect on BDFE. To span electronic effects, CF₃ (electron withdrawing) and NH₂ (electron donating) were chosen as the substituents. Despite the large difference in Hammett constants ($\sigma = XX$). The calculated Mo(PY5-X) BDFEs can be seen in Table S4. Both modified complexes show decreased BDFEs.

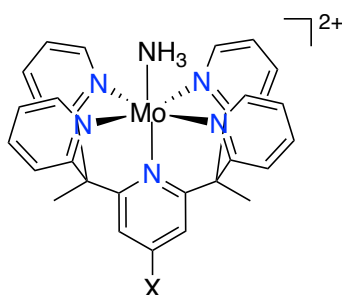


Figure S3. Modified PY5-X ligand, where X = NH₂, H, and CF₃

Table S4. Modified PY5 ligands and their BDFEs

PY5-X	First BDFE	Second BDFE	Third BDFE
NH ₂	62.2	63.8	64.7
H	68.1	64.8	64.0
CF ₃	61.2	59.8	63.7

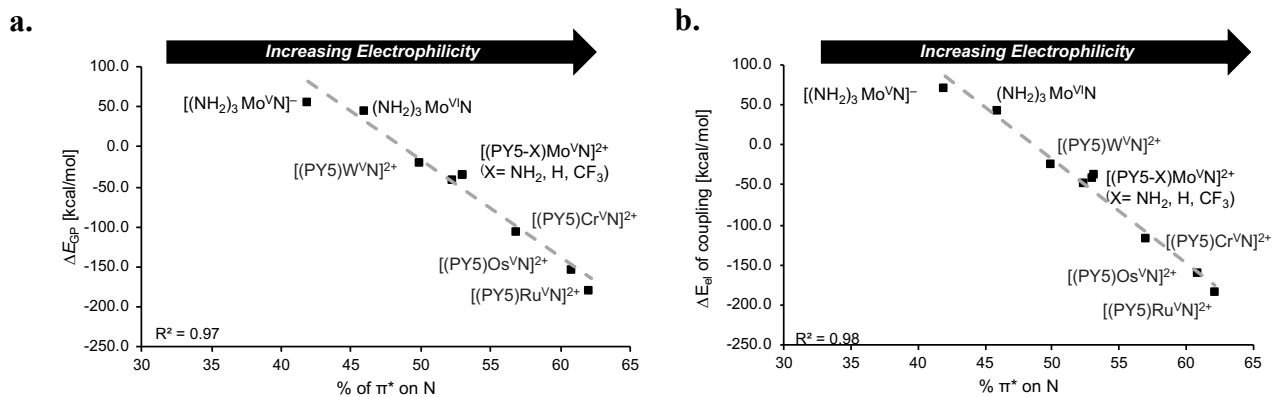


Figure S4. a. Gas-phase electronic energy change and b. Solution phase electronic energy for the coupling vs. the amount of π^* character of the nitride ligand.

In Figure S4a, we see the gas phase electronic energy (ΔE_{GP}) and b. the solution phase electronic energy of equation 1 plotted as a function of the amount of π^* on the nitrido. Within the Mo-based complexes, we can decouple the effects of oxidation state, geometry, and ligand identity. The effect of the metal oxidation state has been analysed by comparing $[(\text{NH}_2)_3\text{Mo}^{\text{VI}}\text{N}]^-$ and $[(\text{NH}_2)_3\text{Mo}^{\text{V}}\text{N}]^-$. The more oxidized the metal, the more nitrido-centred the π^* orbitals are. Consequently, Mo^{VI} nitrido is more electrophilic than Mo^{V} nitrido). In the octahedral PY5 systems, the π^* orbitals shift from metal- to ligand-centred, with 53% of π^* orbital residing on the nitrido. The electronic energy change, ΔE_{el} , for reaction 4 scales accordingly. This observation indicates that the favourable coupling in the Mo complexes is linked to symmetry effects. The more reactive (PY5)Ru nitrido features 62% of the π^* orbital on the nitrido and a correspondingly favourable ΔE_{el} . However, it also features significant radical character on the nitrido. This is more in line with an oxidation state assignment of Ru^{IV} . The ability of $[(\text{PY5})\text{MoN}]^{2+}$ to engage in N–N bond formation is taken as a further indication possible NH_3 oxidation activity. Mn appears to be an outlier in this group. The otherwise strong correlation here ($R^2 > 0.95$ without Mn), coupled with the constant ΔG of NH_3 binding across metals (see main text), implies that the electrophilicity of the nitrido is a major driving force in N–N coupling.

Table S5. All reported complexes, their π^* character, solution phase formation of the $\mu\text{-N}_2$ complexes, and electronic and solution phase energies to couple and evolve N_2 .

Complex	% π^* on N	ΔE_{el} kcal/mol	ΔE_{GP} (eq. 1) kcal/mol	ΔE_{el} (eq. 1) kcal/mol
$[(\text{NH}_2)_3\text{Mo}^{\text{V}}\text{N}]^-$	46.0	24.6	33.9	44.0
$(\text{NH}_2)_3\text{Mo}^{\text{VI}}\text{N}$	42.0	81.2	23.7	55.2
$[(\text{PY}5)\text{Cr}^{\text{V}}\text{N}]^{2+}$	57.0	53.4	-81.4	-106.9
$[(\text{PY}5)\text{Mo}^{\text{V}}\text{N}]^{2+}$	52.3	102.7	-25.8	-42.0
$[(\text{PY}5)\text{W}^{\text{V}}\text{N}]^{2+}$	50.0	108.0	-15.2	-20.1
$[(\text{PY}5)\text{Fe}^{\text{V}}\text{N}]^{2+}$	0.0	-31.3	-167.7	-208.8
$[(\text{PY}5)\text{Ru}^{\text{V}}\text{N}]^{2+}$	62.2	-13.5	-155.4	-179.3
$[(\text{PY}5)\text{Os}^{\text{V}}\text{N}]^{2+}$	60.9	0.0	-130.1	-155.4
$[(\text{CF}_3\text{-PY}5)\text{Mo}^{\text{V}}\text{N}]^{2+}$	53.1	--	--	-36.8
$[(\text{NH}_2\text{-PY}5)\text{Mo}^{\text{V}}\text{N}]^{2+}$	53.1	--	--	-35.2
$[\text{Cp}(\text{P}^{\text{Ph}}_2\text{N}^{\text{tBu}}_2)\text{Mo}^{\text{V}}\text{N}]^+$	48.3	-15.3	-32.1	--

Geometries

Geometries for all compounds discussed in this work can be found in the accompanying XYZ file. This can be opened with free software like MacmolPLT or Mercury, which can be found online. (<https://www.ccdc.cam.ac.uk/mercury/>).

Experimental Procedures

General Considerations:

All manipulations were performed using either glovebox or Schlenk techniques. All glassware was oven dried. Acetonitrile- d_3 (99.8% D) and $^{15}\text{NH}_3$ (98% purity) were purchased from Cambridge Isotope Laboratories, Inc. and the ammonia was used as received. 1,2-difluorobenzene, THF, and diethyl ether were purchased from Fischer Scientific and purified before use. THF and diethyl ether were purified by passage through a neutral alumina column using an Innovative Technology, Inc., PureSolv™ solvent purification system. THF was further dried over sodium/potassium amalgam (NaK) and diethyl ether was further dried over sodium benzophenone with the addition of 1-2 mL/L tetraglyme; both were then distilled and stored over activated 4 Å molecular sieves. 1,2-difluorobenzene and acetonitrile- d_3 were dried over 4 Å molecular sieves for 24 hrs followed by stirring over P_2O_5 (1% wt/vol) for 24 hours, then distilled and stored over activated 4 Å molecular sieves. AgOTf was purchased from Sigma-Aldrich and recrystallized under inert atmosphere by addition of hexanes into a concentrated C_6H_6 solution, then dried by heating to 60 °C under vacuum (1×10^{-5} torr) for 12 hours away from ambient light. $\text{MoI}_2(\text{CO}_3)(\text{MeCN})_2$,¹⁶ 2,6-bis(1,1-di(pyridin-2-yl)ethyl)pyridine (Py_5Me_2),¹⁷ and 2,4,6-tri-*tert*-butylphoxyl radical¹⁸ were synthesized according to literature procedures. NMR spectra were acquired using an INOVA 500 MHz spectrometer. ^1H NMR chemical shifts are reported relative to acetonitrile- d_3 (δ 1.94). ^{15}N NMR chemical shift were referenced to an external $\text{CH}_3^{15}\text{NO}_2$ standard (δ 0.00). NMR spectra were processed using MNova 10.0.

Headspace gas analysis was performed using an Agilent Technologies 6850 GC System equipped with a Supelco 10 ft x 1/8 inch carbosieve column with a thermal conductivity detector (TCD). The method for gas analysis was performed with the following parameters: Inlet temperature: 230 °C; Flow: 15.9 mL/min; Oven temperature and ramp program: initial temperature 40 °C, hold 12 minutes; 40 °C/min to 200 °C.; Carrier gas: Ar; Detector: TCD at 250 °C.

UltraHigh Purity He gas (99.999%) was used as an internal standard for N_2 quantification. An ultrapure research grade premixed primary gas standard of H_2 (0.499%), He (0.499%), N_2 (4.999%), and Ar (94.003%) was purchased from RedBall Oxygen. The gas response factors for N_2 , H_2 , and He were determined from injecting 0.10-0.20 mL of the calibration gas and running the GC method described above. The He response was normalized to 1.0, N_2 and H_2 response factors were determined to be 0.21 and 1.25 respectively for this gas quantification method. The gas retention times of He, H_2 , N_2 are 1.1, 1.8 and 8.2 min, respectively. Oxygen and nitrogen could be nearly resolved thus O_2 and N_2 contaminants from air that were introduced during sample injection were subtracted assuming an air composition of 20.95% O_2 and 78.09% N_2 .

Synthetic Procedures:

1. $[Mo(Py_5Me_2)I]I_2$: This is a modified literature procedure.¹⁹ A 100 mL round bottom flask charged with $MoI_2(CO_3)(MeCN)_2$ (956 mg, 1.85 mmol), toluene (30 mL), and Py_5Me_2 (552 mg, 1.24 mmol) was heated to reflux under nitrogen for 68 hours. After removal of all volatiles the resulting brown powder was taken up into CH_3CN (*ca.* 240 mL) and stirred for 48 hours to fully dissolve the product. The mixture was then filtered through a fine porosity fritted filter. The product was then precipitated from solution with Et_2O (*ca.* 200 mL). $[Mo(Py_5Me_2)I]I_2$ was then filtered, washed with Et_2O (50 mL), and collected as a bright orange powder (446 mg, 39%). 1H NMR (CD_3CN , 500 MHz, 295K) δ -81.37 (1H, $\nu^{1/2} = 130$ Hz), -71.67 (4H, $\nu^{1/2} = 118$ Hz), -54.96 (4H, $\nu^{1/2} = 965$ Hz), -7.40 (6H, $\nu^{1/2} = 165$ Hz), 36.03 (4H, $\nu^{1/2} = 64$ Hz), 60.05 (4H, $\nu^{1/2} = 130$ Hz), 63.57 (2H, $\nu^{1/2} = 100$ Hz).
2. $[Mo(Py_5Me_2)OTf](OTf)_2 \cdot THF$: This is a modified literature procedure.¹⁹ A solution of $AgOTf$ (386 mg, 1.5 mmol) in CH_3CN (9 mL) was added dropwise to a schlenk bomb charged with $[Mo(Py_5Me_2)I]I_2$ (446 mg, 0.485 mmol) and CH_3CN (9 mL). The reaction vessel was sealed and the resulting light green suspension was heated to 60 °C for 15 hours. The reaction mixture was then cooled to 23 °C, concentrated to *ca.* 3 mL, filtered, and washed with CH_3CN (2 mL). The product was crystallized by vapor diffusion of THF into the CH_3CN solution for 72 hours. $[Mo(Py_5Me_2)OTf](OTf)_2 \cdot THF$ was collected as a pale-green crystalline solid (415 mg, 81 %). 0.5-1% of $[Mo(Py_5Me_2)O](OTf)_2$ was often present in the recrystallized material, but can be removed by fractional recrystallized as described above. 1H NMR (CD_3CN , 500 MHz, 295K) δ -78.54 (1H, $\nu^{1/2} = 550$ Hz), -68.00 (4H, $\nu^{1/2} = 470$ Hz), -7.49 and -6.7 (8H, overlapping, $\nu^{1/2} = 2668$ Hz), 1.83 (4H, m, THF), 3.67 (4H, m, THF) 37.06 (6H, $\nu^{1/2} = 226$ Hz), 50.71 (4H, $\nu^{1/2} = 315$ Hz), 68.77 (2H, $\nu^{1/2} = 354$ Hz).
3. $[Mo(Py_5Me_2)OTf](OTf)$: This is a modified literature procedure.¹⁹ To a 50 mL round bottom flask charged with $[Mo(Py_5Me_2)OTf](OTf)_2 \cdot THF$ (260 mg, 0.24 mmol) and KC_8 (33 mg, 0.24 mmol) was added THF (*ca.* 20 mL) at -78 °C. The resulting deep purple solution was allowed to slowly warm to room temperature over the course of 3 hours then all volatiles were removed under vacuum. The resulting dark green solid was taken up into 1,2-difluorobenzene (10 mL) and filtered through a fine porosity fritted filter. The filter cake was washed with an additional 35 mL of 1,2-difluorobenzene. The product was recrystallized by vapor diffusion of Et_2O into the concentrated 1,2-difluorobenzene solution for 72 hours. $[Mo(Py_5Me_2)OTf](OTf)$ was obtained as a dark green crystalline solid (76 mg, 37 %). 1H NMR (CD_3CN , 500 MHz, 295K) δ -62.46 (4H, $\nu^{1/2} = 68$ Hz), -42.81 (4H, $\nu^{1/2} = 33$ Hz), 4.66 (6H, $\nu^{1/2} = 576$ Hz), 31.81 (4H, $\nu^{1/2} = 29$ Hz), 34.03 (4H, $\nu^{1/2} = 26$ Hz), 38.61 (2H, $\nu^{1/2} = 32$ Hz), 62.42 (1H, $\nu^{1/2} = 47$ Hz).

General procedure for N₂ forming reactions and headspace analysis:

In an N₂ filled glove box, a J. Young NMR tube was charged with 0.75 mL of a 19.04 mM stock solution of [Mo(Py₅Me₂)OTf]OTf in acetonitrile-*d*₃. The NMR tube was sealed, then degassed by freeze-pump-thaw cycles (3×). The tube was then charged with 1 atmosphere of ¹⁵NH₃, carefully tapped to assist with gas/liquid mixing for 30 seconds, and then the tube was sealed. The tube was then removed from the Schlenk line and mixed for an additional 30 seconds using a vortex mixer. After complete mixing the NMR tube was brought into an Argon filled glove box, quickly opened and charged with solid 2,4,6-tri-*tert*-butylphenoxy radical 80 mg (0.31 mmol), then immediately sealed. The tube was shaken, then placed into an NMR spectrometer to collect a ¹⁵N NMR spectrum of the reaction mixture for 18 hours.

After collection of the ¹⁵N NMR spectrum, the J. Young tube was attached to the gas sampling apparatus (Figure S10-S11). The headspace above the tube was evacuated and sealed off from vacuum, then the J. Young tube was opened. He gas (0.2 mL) was injected into the gas sampling apparatus, mixed into the reaction headspace by withdrawing 0.8 mL into the syringe and reinjected every 30 seconds for 2 minutes. The headspace was allowed to equilibrate for an additional minute, then the head space was removed using the gas tight syringe, sealed, and injected into the GC for analysis.

To account for any background N₂ production or contamination from the argon glove box used during sample preparation, a control sample was also prepared in the same fashion as described above. Control reaction tubes were prepared in tandem with the reaction tubes, and their headspace was also sampled after 18 hours.

NMR Spectra

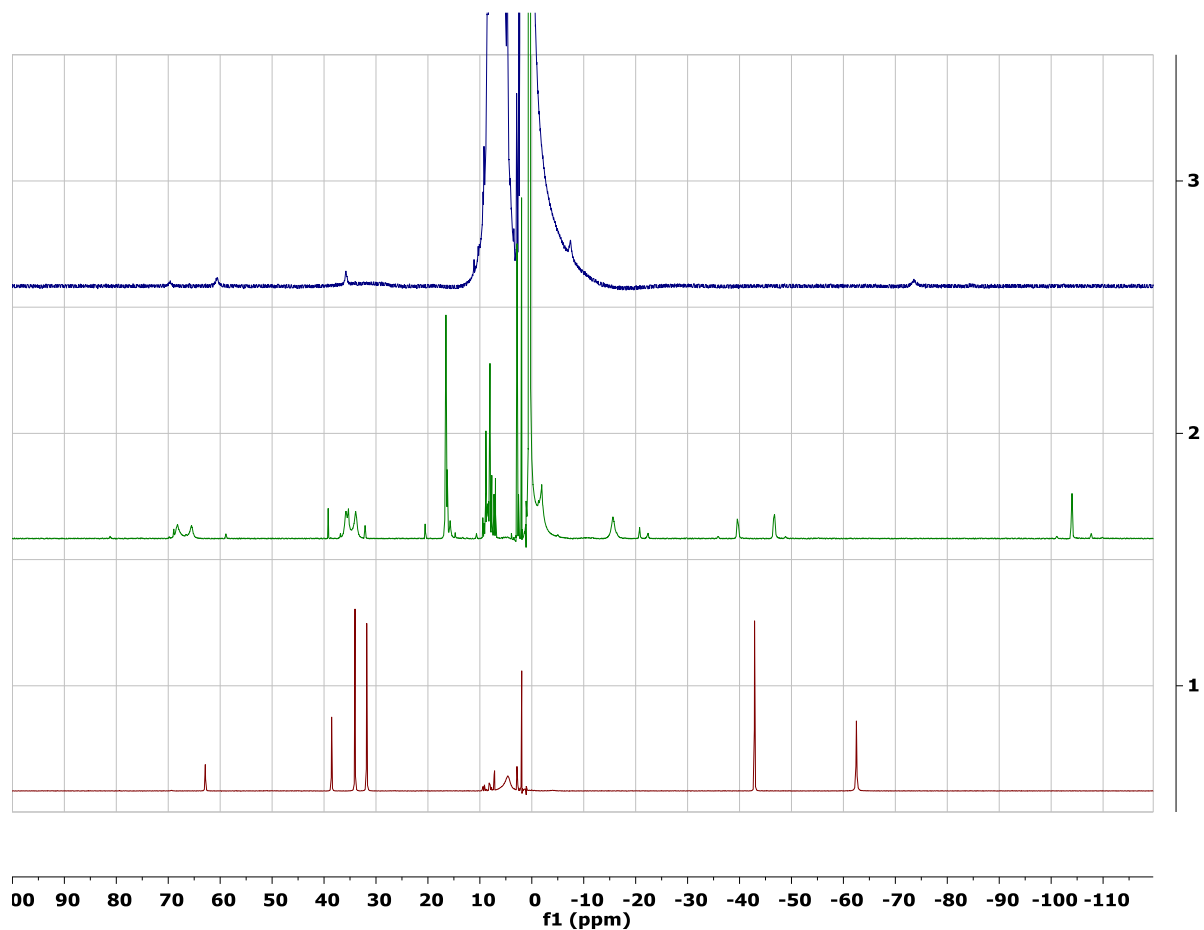


Figure S5. Stacked ¹H NMR spectra of [Mo(Py₅Me₂)OTf]OTf (bottom), after addition of 1 atm of ¹⁵NH₃ (middle), and after addition of 2,4,6-tri-*tert*-butylphenoxy radical (top).

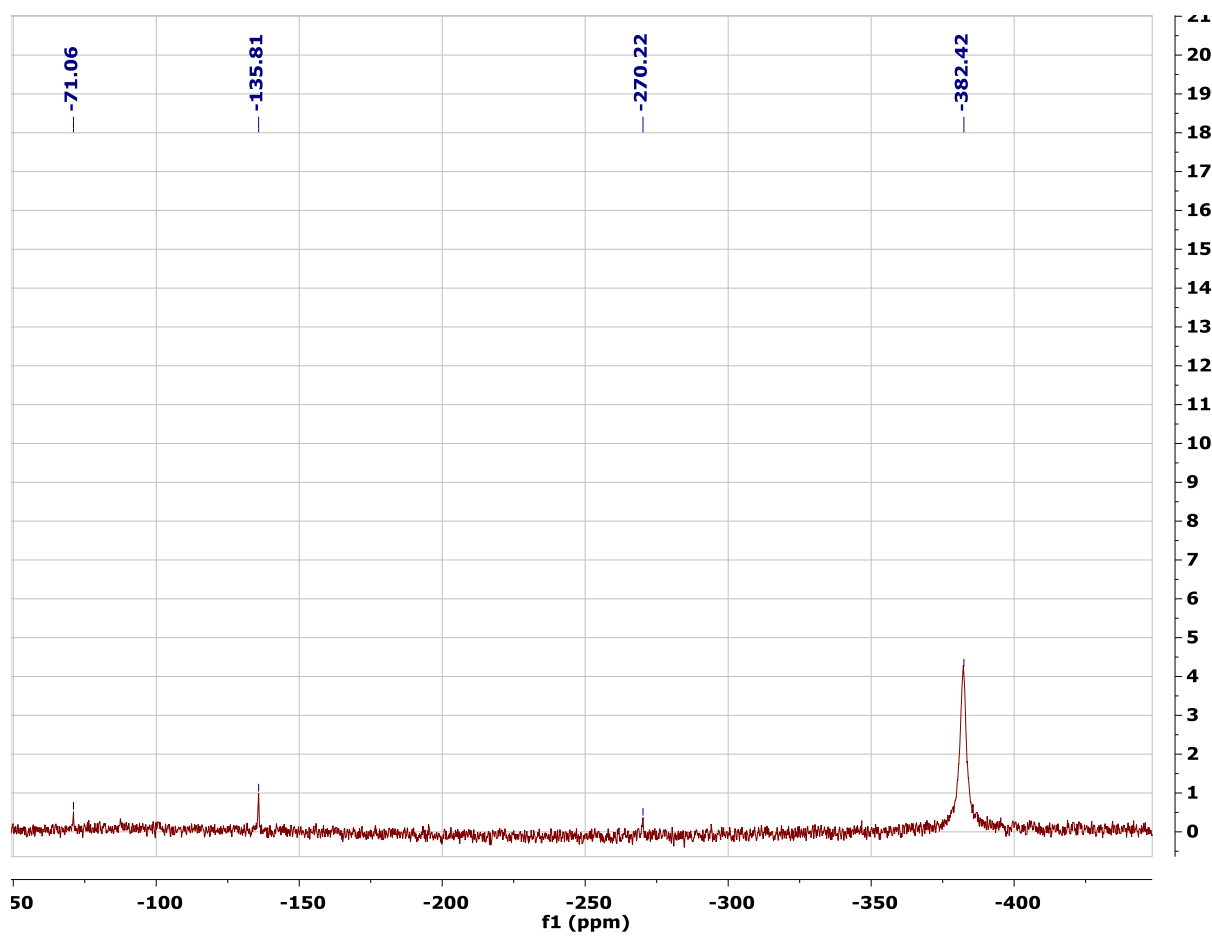


Figure S6. $^{15}\text{N}\{^1\text{H}\}$ NMR spectrum of trial 1 reaction mixture. (CD_3CN , 50.6 MHz, 295 K) δ - 382.42 ($^{15}\text{NH}_3$), -270.22 (unknown), -135.81 (CD_3CN solvent), -71.06 ($^{15}\text{N}_2$).

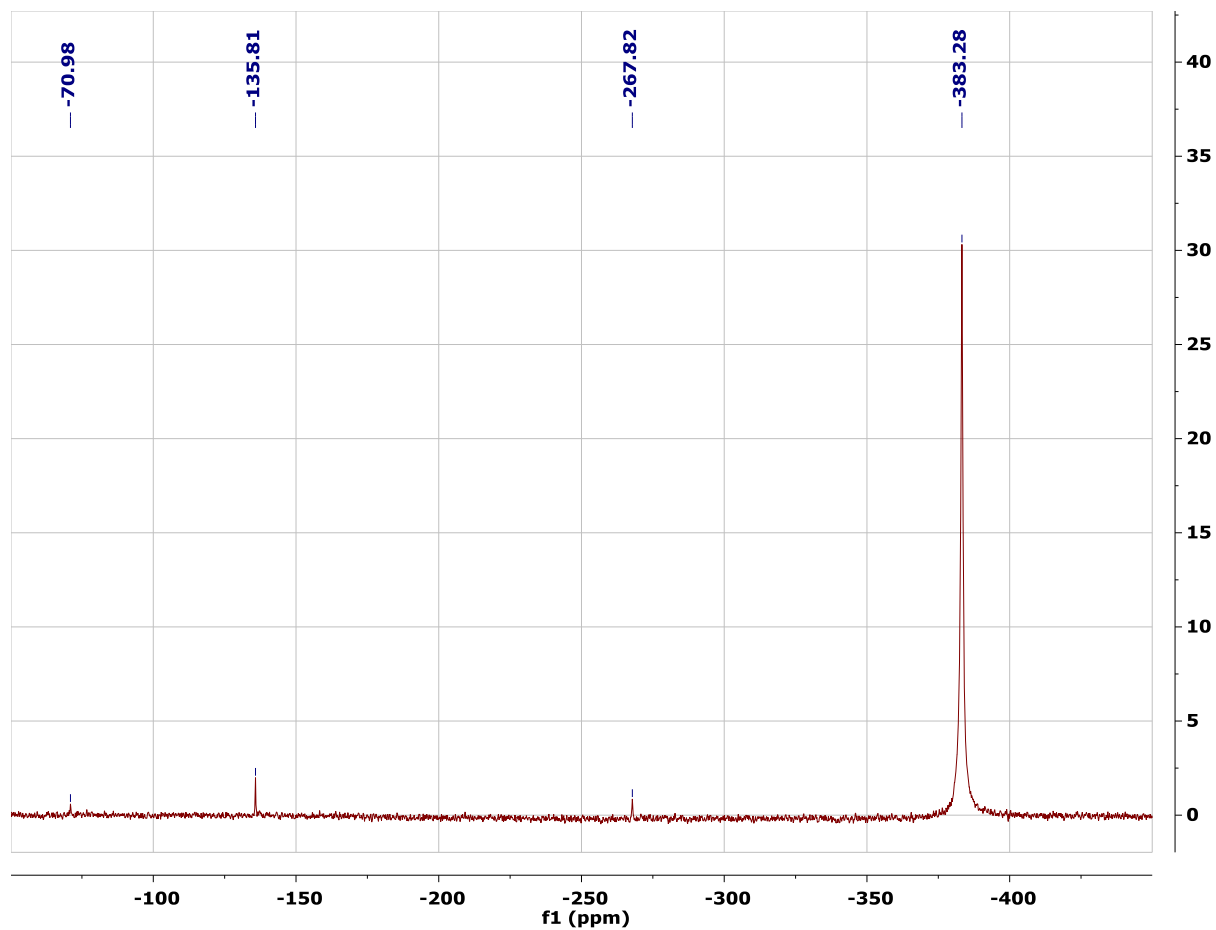


Figure S7. $^{15}\text{N}\{^1\text{H}\}$ NMR spectrum of trial 2 reaction mixture. (CD_3CN , 50.6 MHz, 295 K)
 δ -383.28 ($^{15}\text{NH}_3$), -267.82 (unknown), -135.81 (CD_3CN solvent), -70.98 ($^{15}\text{N}_2$).

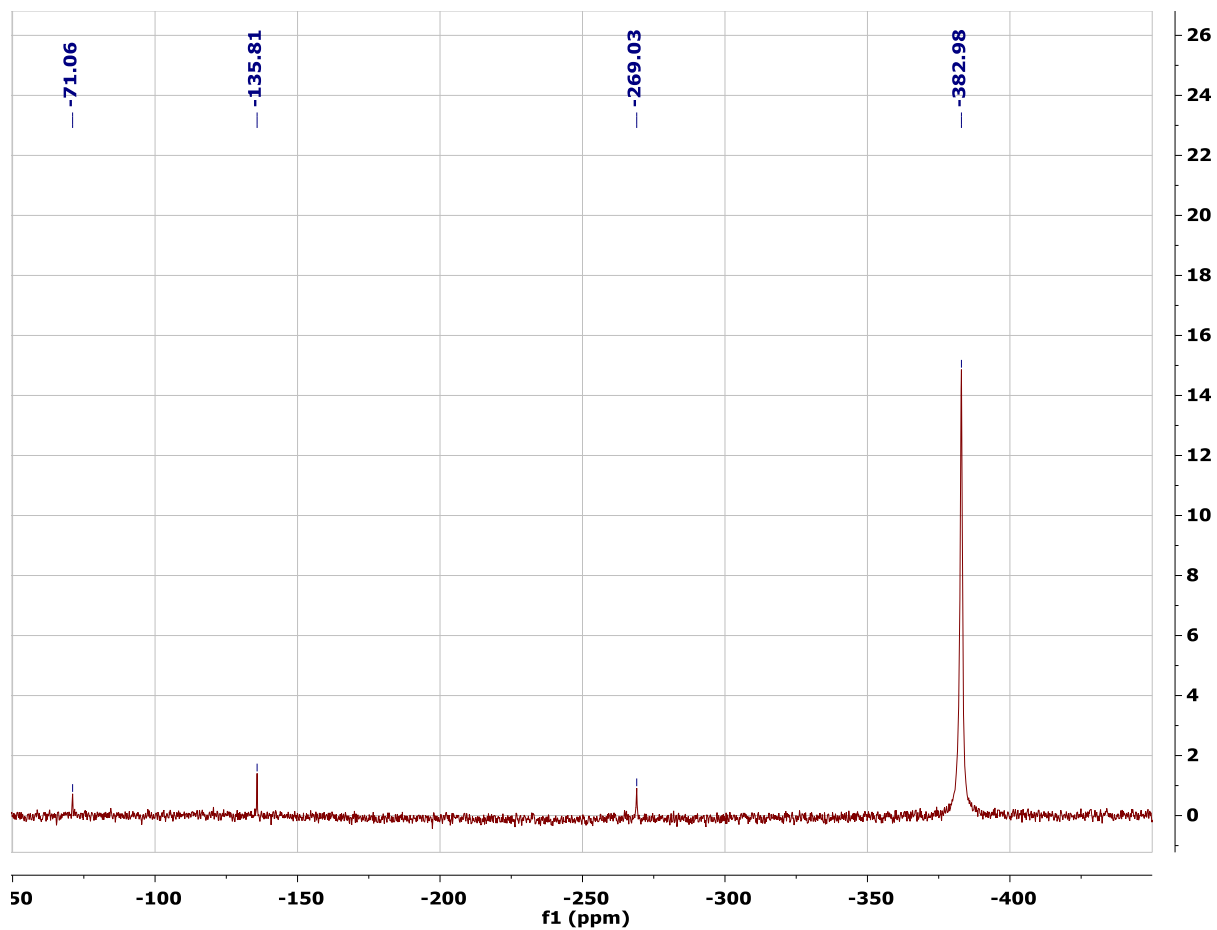


Figure S8. $^{15}\text{N}\{^1\text{H}\}$ NMR spectrum of trial 3 reaction mixture. (CD_3CN , 50.6 MHz, 295 K) δ - 382.98 ($^{15}\text{NH}_3$), -269.03 (unknown), -135.81 (CD_3CN solvent), -71.06 ($^{15}\text{N}_2$).

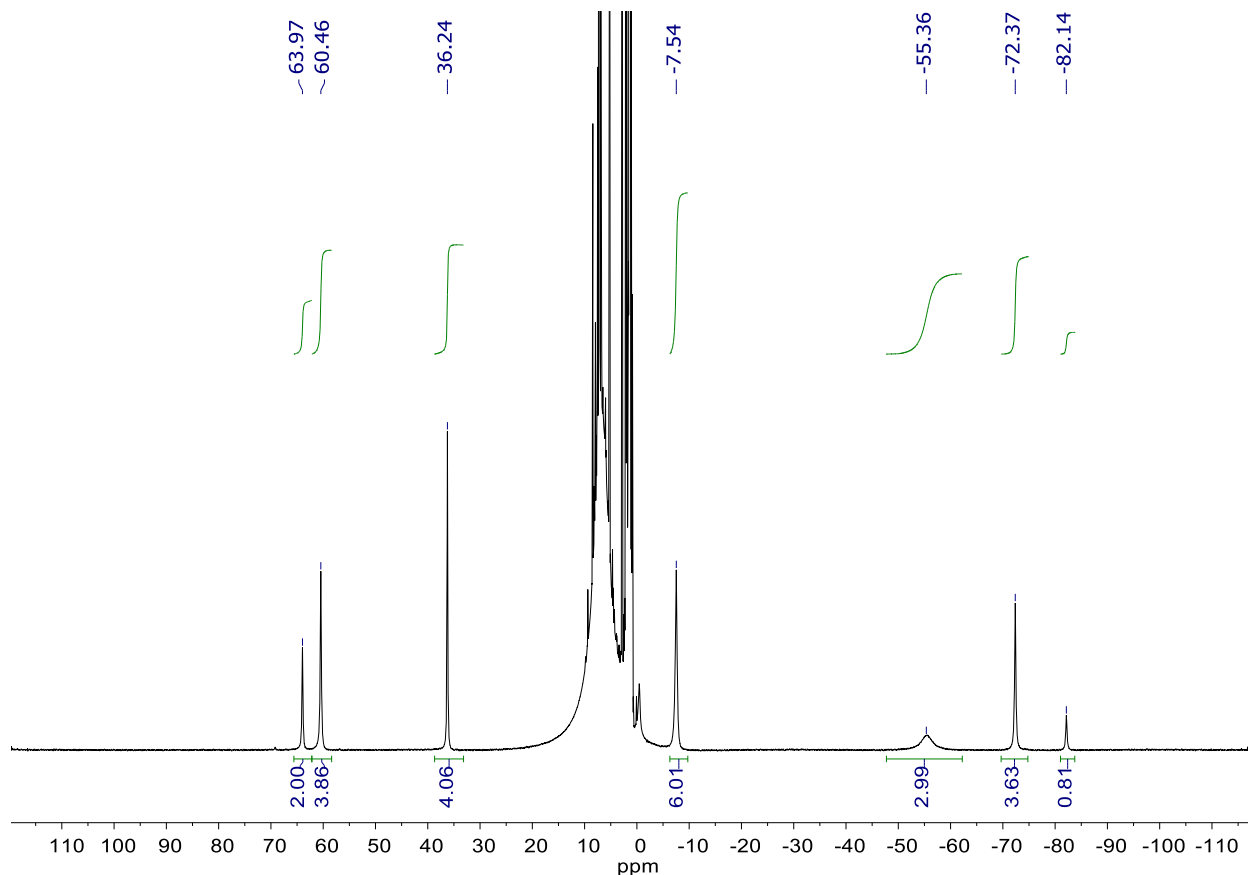


Figure S9. ^1H NMR spectrum of the reaction between $[\text{Mo}(\text{Py}_5\text{Me}_2)\text{OTf}]\text{OTf}$ and 10 equiv 2,4,6-tri-*tert*-butylphenoxy radical in CD_3CN . The chemical shifts of the paramagnetic resonances are similar to those of $[\text{Mo}(\text{Py}_5\text{Me}_2)\text{I}]\text{I}_2$, suggesting the product may be a $[\text{Mo}(\text{Py}_5\text{Me}_2)(\text{OAr})](\text{OTf})_2$.



Figure S10. Disassembled apparatus for J.Young tube headspace sampling.



Figure S11. Apparatus for J.Young tube headspace sampling with gas tight syringe.

Gas Chromatograms

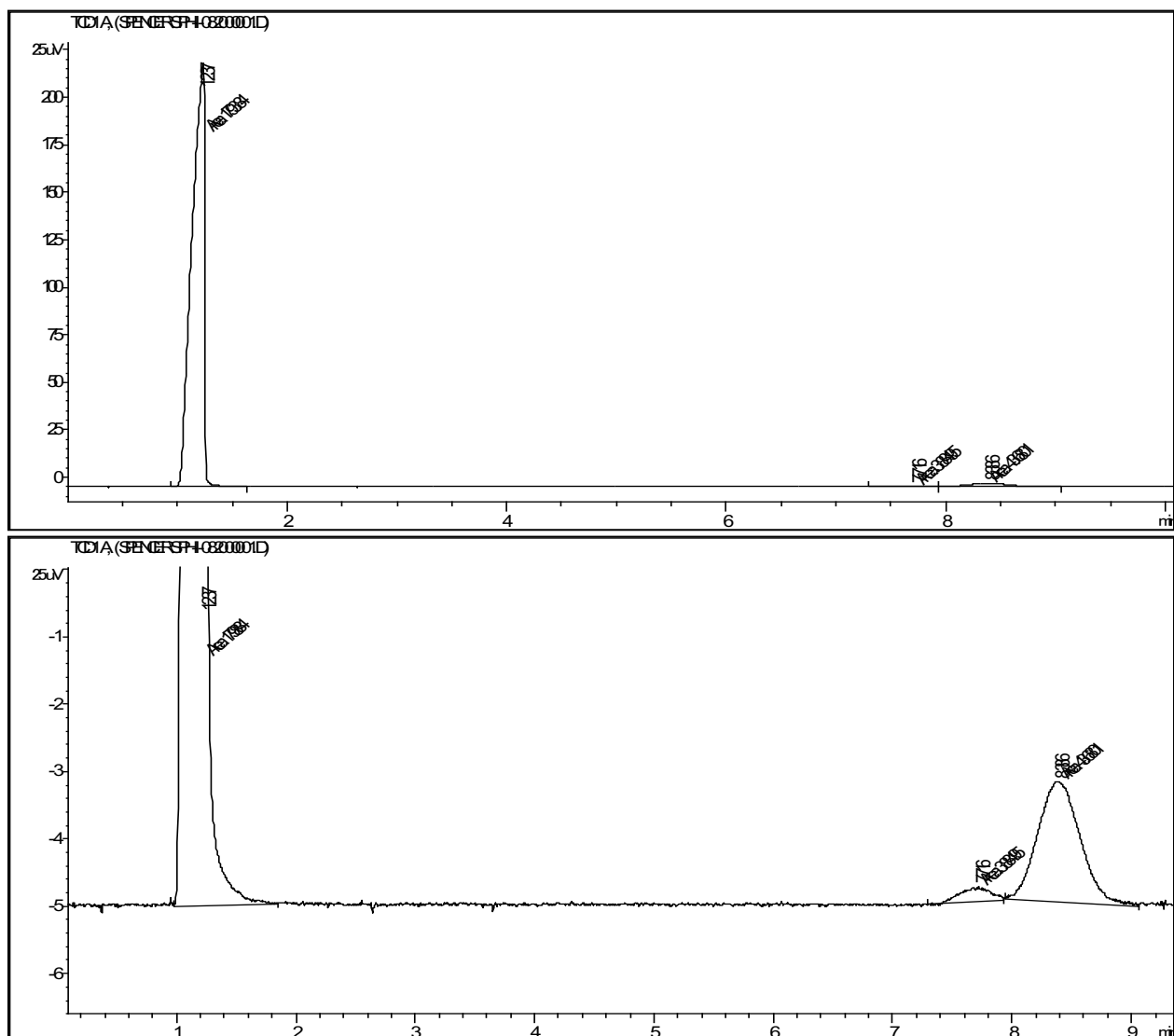


Figure S12. Chromatogram of trial 1 control reaction headspace without [Mo(Py₅Me₂)OTf]OTf. Expanded view (top) and zoomed in view (bottom).

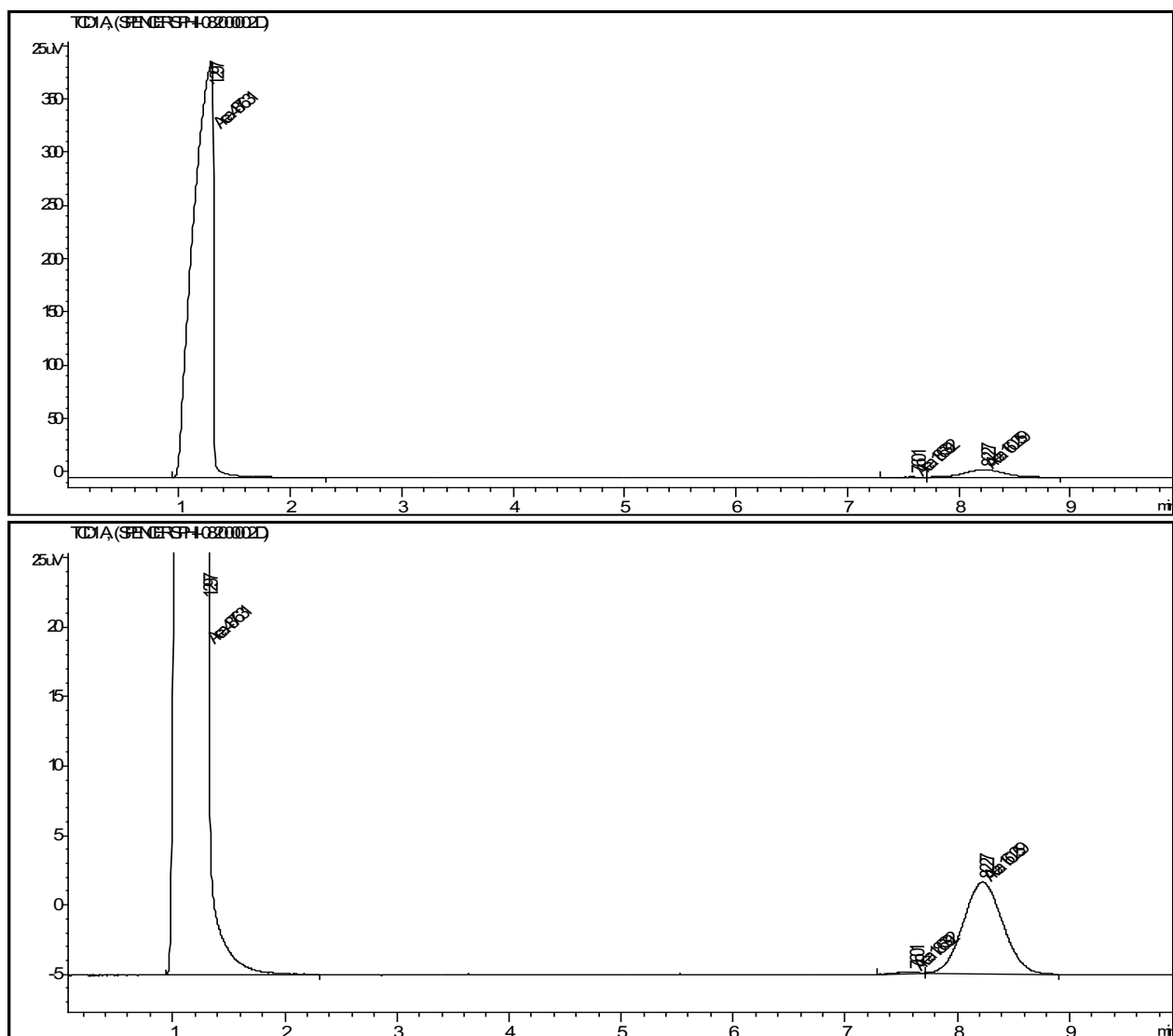


Figure S13. Chromatogram of trial 1 reaction headspace containing $[\text{Mo}(\text{Py}_5\text{Me}_2)\text{OTf}]\text{OTf}$. Expanded view (top) and zoomed in view (bottom).

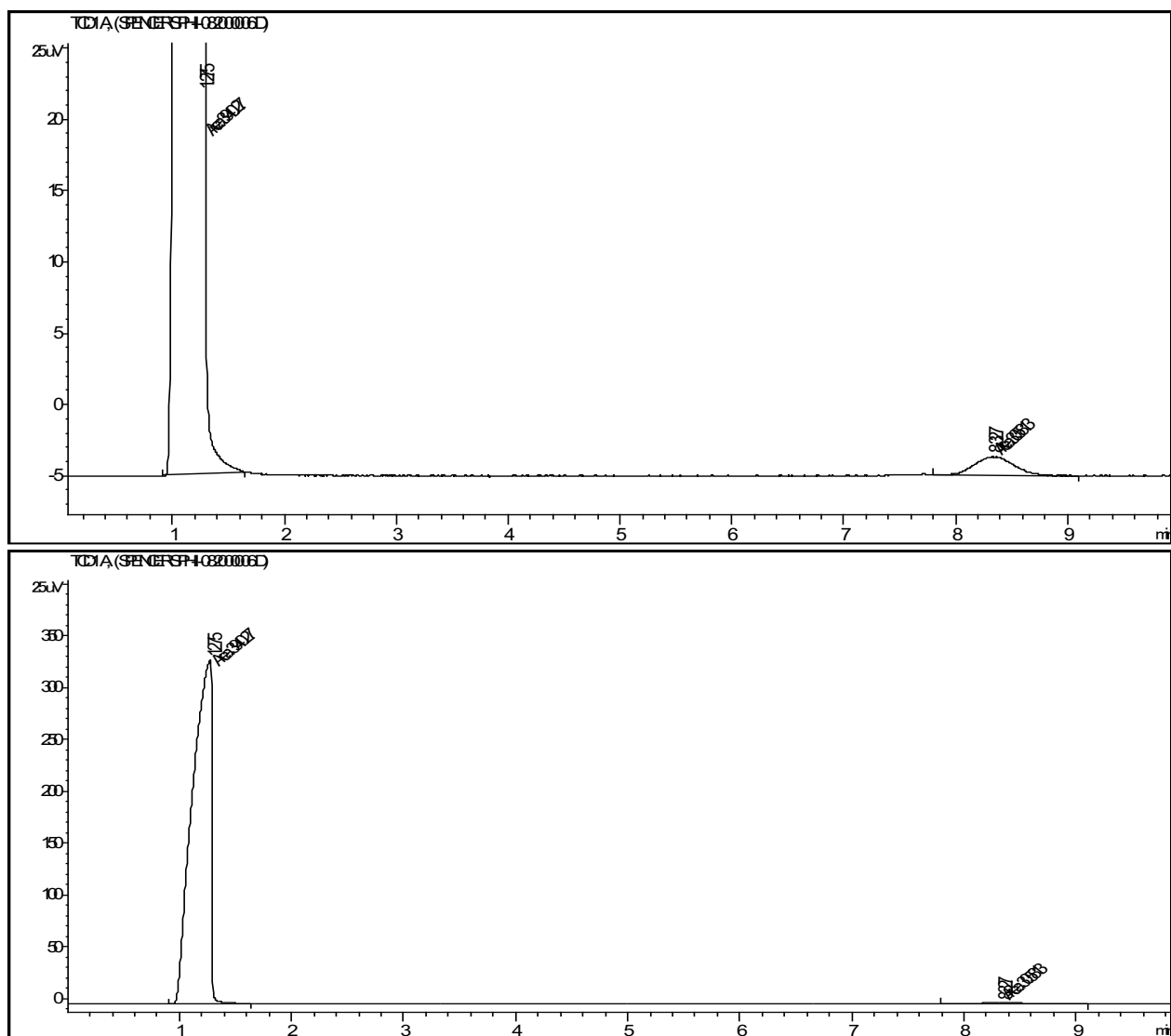


Figure S14. Chromatogram of trial 2 control reaction headspace without Mo(Py₅Me₂)OTf]OTf. Expanded view (top) and zoomed in view (bottom).

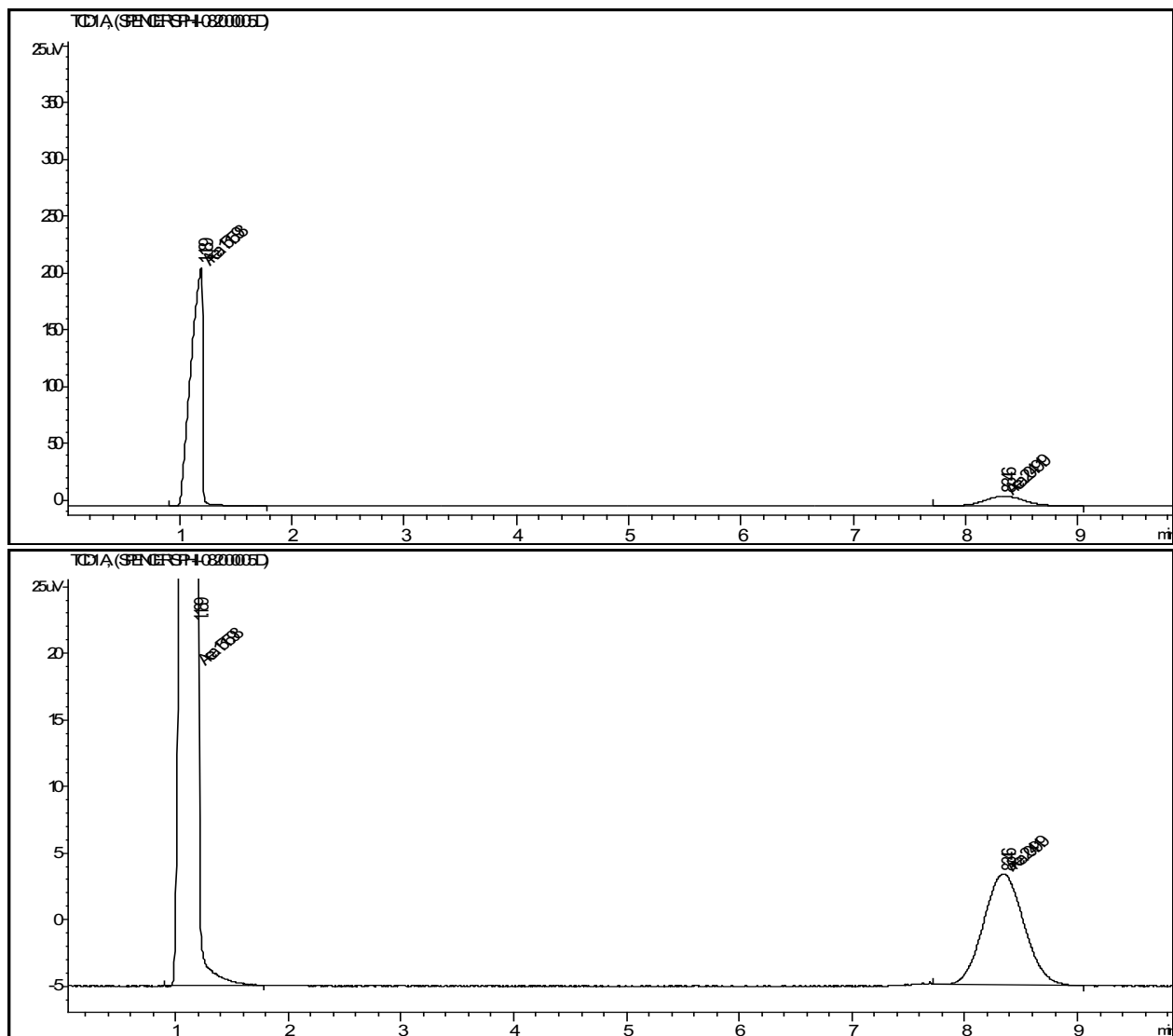


Figure S15. Chromatogram of trial 2 reaction headspace containing $[\text{Mo}(\text{Py}_5\text{Me}_2)\text{OTf}]\text{OTf}$. Expanded view (top) and zoomed in view (bottom).

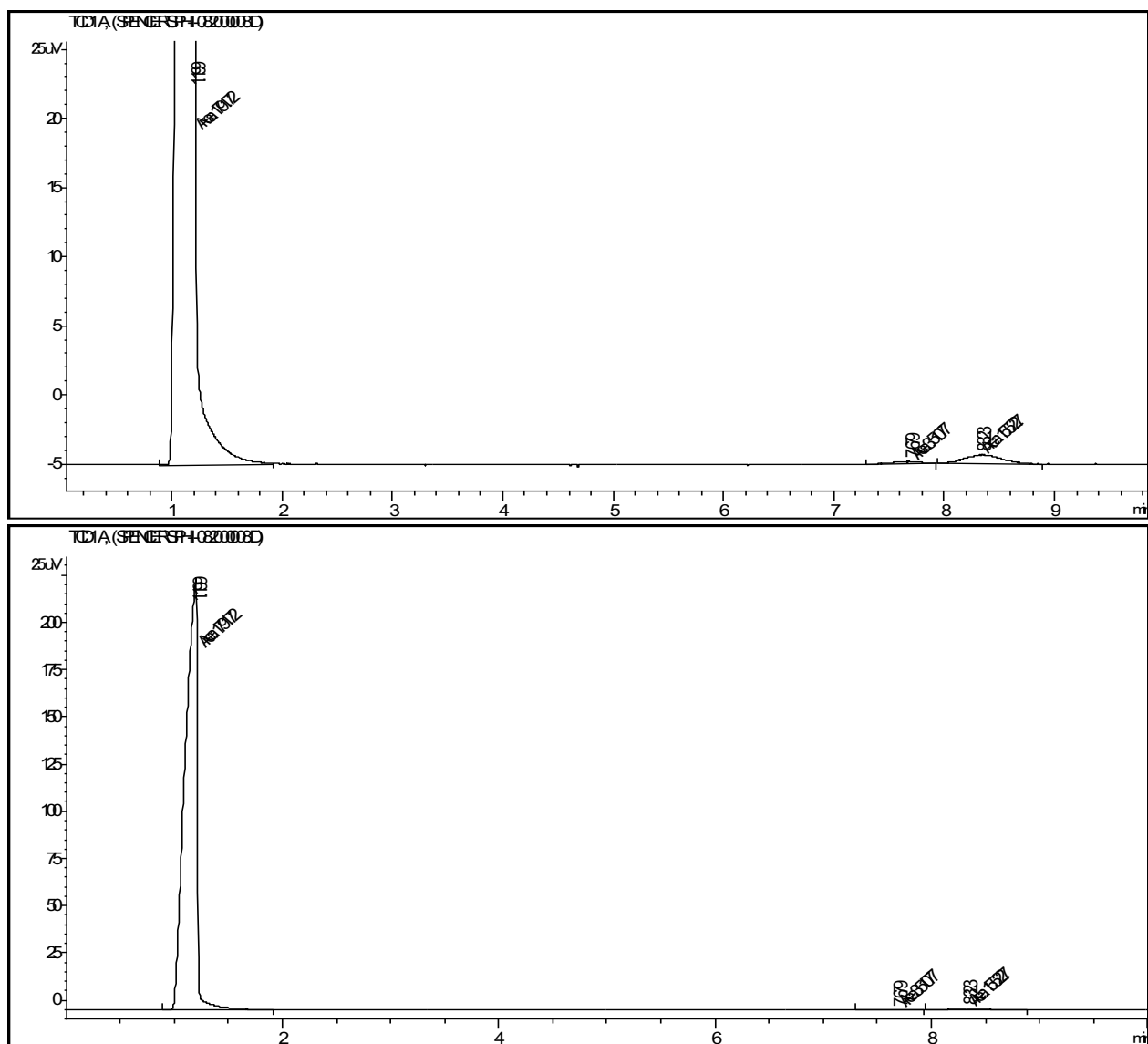


Figure S16. Chromatogram of trial 3 control reaction headspace without $[\text{Mo}(\text{Py}_5\text{Me}_2)\text{OTf}]\text{OTf}$. Expanded view (top) and zoomed in view (bottom).

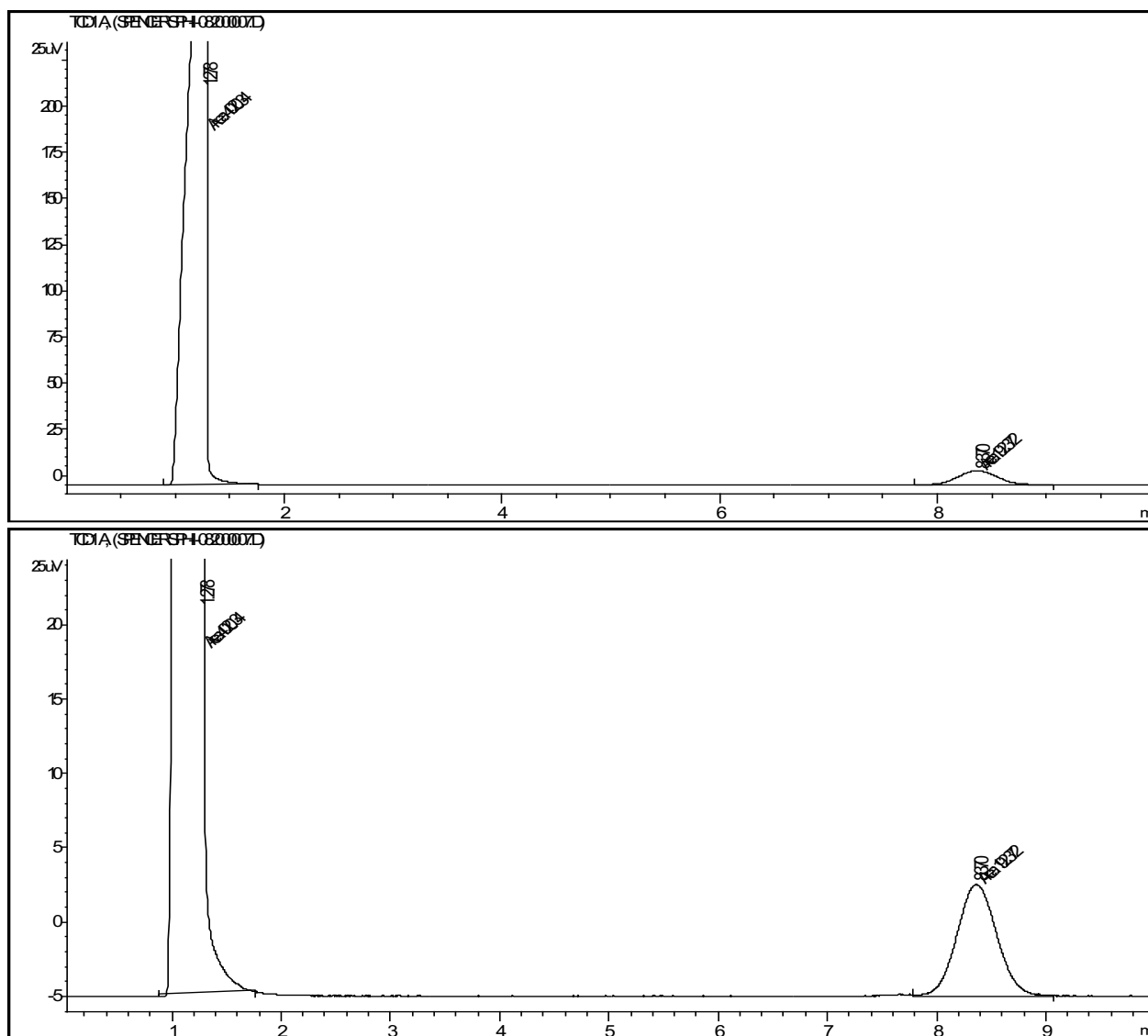


Figure S17. Chromatogram of trial 3 reaction headspace containing $[\text{Mo}(\text{Py}_5\text{Me}_2)\text{OTf}]\text{OTf}$. Expanded view (top) and zoomed in view (bottom).

Results of N₂ Quantification

	Moles N ₂ formed in control reactions (*10 ⁻⁶)	Moles N ₂ formed in reaction (*10 ⁻⁶) ^a	Equivalents of N ₂ ^b
Trial 1	0.6	1.0	0.1
Trial 2	0.3	4.5	0.3
Trial 3	0.1	1.8	0.1
Ave	0.3	2.4	0.2
σ	0.3	1.8	0.1

Table S6. Summary of GC headspace analyses. Control reactions were performed in the absence of [Mo(Py₅Me₂)OTf](OTf). ^a Corrected for air contamination and background N₂ formation.

^b Equivalents of N₂ with respect to [Mo(Py₅Me₂)OTf](OTf).

References

1. A. D. Becke, *J. Chem. Phys.*, 1993, **98**, 5648-5652.
2. C. T. Lee, W. T. Yang and R. G. Parr, *Phys. Rev. B*, 1988, **37**, 785-789.
3. M. M. Francl, W. J. Pietro, W. J. Hehre, J. S. Binkley, M. S. Gordon, D. J. Defrees and J. A. Pople, *Journal of Chemical Physics*, 1982, **77**, 3654-3665.
4. W. J. Hehre, Ditchfie.R and J. A. Pople, *J. Chem. Phys.* , 1972, **56**, 2257-&.
5. D. Andrae, U. Häußermann, M. Dolg, H. Stoll and H. Preuß, *Theo. Chem. Acc*, 1990, **77**, 123-141.
6. S. Grimme, *J. Comp. Chem.* , 2006, **27**, 1787-1799.
7. A. V. Marenich, C. J. Cramer and D. G. Truhlar, *J. Phys. Chem. B*, 2009, **113**, 6378-6396.
8. O. C. Bridgeman, Aldrich, E.W., , *J. Heat Transfer*, 1964, **86**, 279-286.
9. M. J. Frisch, G. W. Trucks, H. B. Schlegel, G. E. Scuseria, M. A. Robb, J. R. Cheeseman, G. Scalmani, V. Barone, B. Mennucci, G. A. Petersson, H. Nakatsuji, M. Caricato, X. Li, H. P. Hratchian, A. F. Izmaylov, J. Bloino, G. Zheng, J. L. Sonnenberg, M. Hada, M. Ehara, K. Toyota, R. Fukuda, J. Hasegawa, M. Ishida, T. Nakajima, Y. Honda, O. Kitao, H. Nakai, T. Vreven, J. A. Montgomery, J. E. Peralta, F. Ogliaro, M. Bearpark, J. J. Heyd, E. Brothers, K. N. Kudin, V. N. Staroverov, R. Kobayashi, J. Normand, K. Raghavachari, A. Rendell, J. C. Burant, S. S. Iyengar, J. Tomasi, M. Cossi, N. Rega, J. M. Millam, M. Klene, J. E. Knox, J. B. Cross, V. Bakken, C. Adamo, J. Jaramillo, R. Gomperts, R. E. Stratmann, O. Yazyev, A. J. Austin, R. Cammi, C. Pomelli, J. W. Ochterski, R. L. Martin, K. Morokuma, V. G. Zakrzewski, G. A. Voth, P. Salvador, J. J. Dannenberg, S. Dapprich, A. D. Daniels, Farkas, J. B. Foresman, J. V. Ortiz, J. Cioslowski and D. J. Fox, *Journal*, 2009.
10. E. D. Glendening, J. K. Badenhoop, A. E. Reed, J. E. Carpenter, J. A. Bohmann, C. M. Morales, C. R. Landis and F. Weinhold, *Journal*, 2013.
11. F. Weigend and R. Ahlrichs, *Phys. Chem. Chem. Phys.*, 2005, **7**, 3297-3305.
12. F. Neese, *Wiley Interdiscip. Rev. Comput. Mol. Sci.*, 2017, **8**, e1327.
13. P. Bhattacharya, Z. M. Heiden, E. S. Wiedner, S. Raugei, N. A. Piro, W. S. Kassel, R. M. Bullock and M. T. Mock, *J. Am. Chem. Soc.*, 2017, **139**, 2916-2919.
14. A. J. Kendall, S. I. Johnson, R. M. Bullock and M. T. Mock, *J. Am. Chem. Soc.*, 2018, **140**, 2528-2536.
15. W. A. Nugent and J. M. Mayer, *Metal-Ligand Multiple Bonds*, Wiley Interscience, New York, 1988.
16. P. K. Baker, S. G. Fraser and E. M. Keys, *J. Organomet. Chem.* , 1986, **309**, 319-321.
17. A. J. Canty, N. J. Minchin, B. W. Skelton and A. H. White, *J. Chem. Soc. Dalton Trans.*, 1986, 2205-2210.
18. V. W. Manner, T. F. Markle, J. H. Freudenthal, J. P. Roth and J. M. Mayer, *Chem. Commun.*, 2008, 256-258.
19. H. I. Karunadasa, C. J. Chang and J. R. Long, *Nature*, 2010, **464**, 1329-1333.